Available online at www.sciencedirect.com
SCIENCE DIRECT
Journal of Power Sources 157 (2006) 181–187
JOURNAL OF POWER SOURCES
www.elsevier.com/locate/jpowsour

Temperature distribution on the MEA surface of a PEMFC with serpentine channel flow bed

Maohai Wang, Hang Guo *, Chongfang Ma

The Key Laboratory of Enhanced Heat Transfer and Energy Conservation, Ministry of Education of China, College of Environmental and Energy Engineering, Beijing University of Technology, No. 100 Pingleyuan, Chaoyang District, Beijing 100022, China

Received 30 April 2005; received in revised form 10 August 2005; accepted 17 August 2005
Available online 21 September 2005

Abstract

Knowledge of the temperature distribution on the membrane electrode assembly (MEA) surface and heat transfer processes inside a proton exchange membrane fuel cell (PEMFC) is helpful to improvement of cell reliability, durability and performance. The temperature fields on the surface of MEA fixed inside a proton exchange membrane fuel cell with a serpentine channel flow bed were measured by infrared imaging technology under non-humidification conditions. The temperature distributions over the MEA surface under whole channel region were achieved. The experimental results show that the downstream temperatures are higher than the upstream. The hot region on the MEA surface is easy to locate from the infrared temperature image. The mean temperature on the MEA surface and the cell temperature both increase with the current density. Higher current density makes the non-uniformity of temperature distribution on the MEA surface worse. The loading time significantly affects the temperature distribution. Compared with the electrical performance of the cell, the MEA's temperatures need much more time to reach stable. The results indicate that isothermal assumption is not appropriate for a modeling of PEMFCs, and monitoring the temperature of external surface of the flow field plate or end plate cannot supply accurate reference to control the temperatures on MEA surface.

Keywords: Proton exchange membrane fuel cells; Membrane electrode assembly; Temperature distribution; Serpentine channel flow bed

1. Introduction

Thermal and fluid processes encountered inside proton exchange membrane fuel cells (PEMFCs) considerably influence the cell performance. Currently, more and more research activities focus on the thermophysical issues inside fuel cells [1]. However, so far, the advances in modeling of the PEMFC have outpaced the ability to experimentally verify the predicted phenomena [2] such as the distributions of various parameters.

Temperature plays a significant role in achieving high performance of fuel cells because it deeply influences the activity of the catalyst, dehydration of solid polymer membrane, mass transfer and heat management of PEMFCs [3]. Even small variations in temperature have dramatic effects on inlet humidity, locations of condensation/vaporization and membrane longevity [4]. The temperature distribution over the membrane electrode assembly (MEA) surface has a close relationship with the performance, lifetime and reliability of PEMFCs. Heat generated in PEMFCs affects the water distribution by increasing temperature and changing the local saturation pressure of the gases. A too high local temperature on MEA surface may lead to membrane dehydration, and a too low temperature may result in water condensation or even flooding. The temperature distribution is of critical importance to water management in a PEMFC. The heat, accompanied with the electrical energy produced by a PEMFC, is required to keep the working temperature of PEMFCs within safe level. Without proper thermal management, the performance of the fuel cell may not be maintained. The temperature is not distributed homogeneously over the active area of the fuel cell [5]. The non-uniform temperature distribution over the MEA surface may decrease the reliability and durability of the membrane applied in PEMFCs. The hot spot should be avoided for the membrane reliability and durability under the operating of PEMFCs. Therefore, determining the temperature field on the MEA surface inside PEMFCs is essential to ensure proper heat management and make the PEMFC work safely.

* Corresponding author. Tel.: +86 10 67391985 8311; fax: +86 10 67392774.
E-mail address: hangguo@sohu.com (H. Guo).

0378-7753/$ – see front matter © 2005 Elsevier B.V. All rights reserved.
doi:10.1016/j.jpowsour.2005.08.012

In addition, knowledge of temperature distribution and heat transport inside fuel cells is helpful to understand distributions of other parameters, to optimize design and operating of fuel cells and to validate the increasingly complicate model of fuel cells.

There is limited modeling and experimental work in the area of temperature distribution on MEA surfaces. Several models had been developed to demonstrate the influence of temperature change on the water management and relationship between temperature and current density by considering the energy equation [6–8]. The temperature distributions along the direction perpendicular to a MEA surface [9–13], as well as the temperature profiles over the membrane surface along a single straight channel [8], were simulated. Recently, experimental studies were conducted to determine the temperature at the electrolyte [14] and the temperature distribution over the MEA surface of an operating PEMFC [4,5,15]. Mench et al. [4] embedded eight micro-thermocouples at different positions within the electrolyte to measure the temperature distribution. Only three thermocouples gave reliable output. The results showed that the electrolyte's temperature rises with the current density. The method is not easy to perform because it is very difficult to prevent the destruction of and interference with the thermocouple embedded in the electrolyte. Hakenjos et al. [5] designed a PEMFC, which permitted simultaneous measurement of current density, temperature distribution and flow field flooding. In that study, infrared imaging technology was used to measure the temperature distribution over a MEA surface. A zinc selenide window was adopted to act as transparent material for infrared light. The authors measured the temperature distribution at the cathode side of the test cell. Locations of liquid water can be confirmed through the images of temperature distributions. The MEA's temperature distributions under partial channel region, not whole channel region, were got because liquid water condensed on the surface of infrared material. The current density loaded to the test cell was less than 0.3 A cm^{-2}. Schimoi et al. [15] applied infrared imaging technology to measure the temperature fields at the MEA's cathode side inside a PEMFC with three parallel channels. Only the temperature data of the center channel region were analyzed because there was liquid water at other channels. From above-mentioned literatures, it is known that so far, all the published experimental results did not wholly demonstrate the temperature distribution over the MEA surface. The effect of loading time on the two-dimensional temperature distribution was also not mentioned in published experimental results.

However, it is necessary to achieve the temperature distribution under whole channel region for locating the hot spot region over the MEA surface, which would accelerate membrane physical degradation and ultimately result in membrane failure [16]. The characteristics of temperature distribution change with current and loading time are also important because they are related to cell operation such as start-up and changing cell load. Knowing the temperature distribution under whole channel region and its change with current and loading time can supply more accurate reference for improvement of cell design and operating, proper water/heat management and validation of numerical models.

In this paper, a new design was presented to measure the MEA's temperature under whole channel region with the infrared imaging technology. The aims of the paper are to achieve the temperature distribution under whole channel region over the MEA surface and to explore the change trend of temperature distribution change with loaded current and loading time.

2. Experimental

Fig. 1 shows the structure of the specially designed test cell for measuring the MEA surface's temperature distribution. A serpentine channel (3 mm channel width, 1.5 mm rib width and 2.5 mm channel depth) was machined through stainless steel plates to form an active cell area of 29 mm × 39 mm. The anode channels were completely broken through to allow a straight view onto the anode surface of the MEA. The reason for taking the anode, not the cathode, side of MEA as the measuring surface is that liquid water emerged at cathode side would lead to untrue temperature distribution over the MEA surface [5,15]. The plates were coated with gold for corrosion protection. A barium fluoride was applied to close the anode gas channels. As barium fluoride is transparent for infrared light, the anode temperature distribution of the MEA could be observed with an infrared thermo tracer. The thermo tracer (NEC, TH5102) is sensitive to a range of infrared wavelength between 8 and 12 μm. Catalyst (Pt/C, 0.8 mg cm^{-2}) was applied onto the gas diffusion layers (carbon paper) with Nafion^{TM} solution. The electrodes were hot-bonded onto a Nafion^{TM} membrane (89 μm thick) so as to be a single sheet.

In order to get more accurate temperature readings, the real emissivity of the measured surface of the MEA should be found. A black body and the MEA were maintained at the same temperature. The window protective cap of the thermo tracer was used as the black body. First, the thermo tracer was used to get the temperature of the black body by setting emmissivity as 1.0. Then, the temperatures of the MEA surface were measured with the thermo tracer at various emmissivities. The emmissivity under which the temperature on MEA surface was equal to that of the black body was considered as the emmissivity of the MEA surface. With the method presented above, the emmissivity of the surface was set as 0.96.

The transmission of the barium fluoride was measured with a Fourier spectrometer (BRUKER, EQUINOX55). Fig. 2 shows the transmission over the sensitive infrared wavelength. The

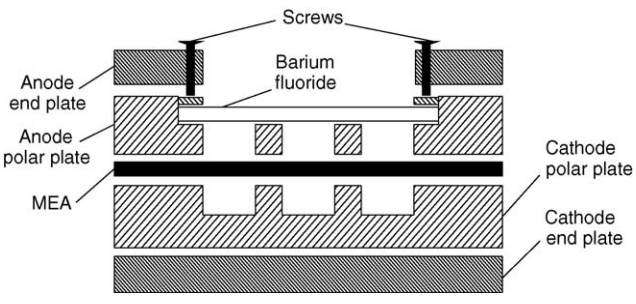

Fig. 1. Structure of the experimental PEMFC.

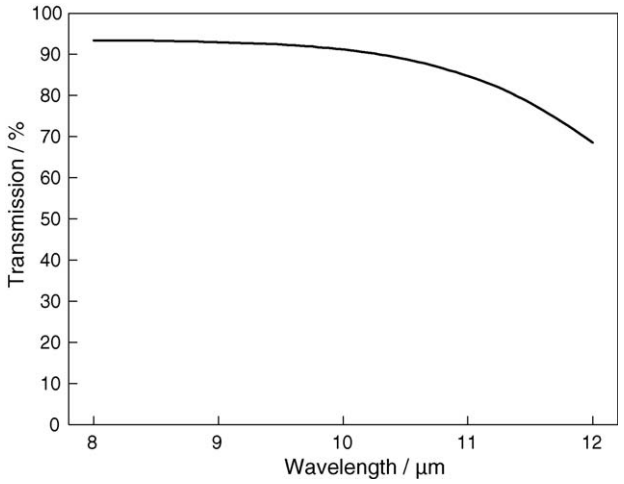

Fig. 2. Fourier spectrogram of the barium fluoride window between 8 and 12 μm.

mean transmission is 87.8%, which is enough for the material to act as an infrared window.

In this case, both the precision of the thermo tracer and the absorption of the barium fluoride result in a measurement error. A calibration was conducted to overcome the problem. The real temperatures measured with a copper constantan thermocouple (0.5 mm diameter of copper and constantan wires) were compared with the temperatures captured by the thermo tracer behind the barium fluoride when the emmissivity was set as 0.96 and a correlation between the two sets of temperature was obtained. The curve and the fitted equation are given in Fig. 3. All the data from Figs. 7–10 were converted with that equation. After conversion, the deviation of the converted temperature against temperature measured with thermocouple was less than ±0.3 °C in the range of 20–80 °C.

The flow rates of hydrogen and oxygen were controlled by mass flow controllers. A temperature and heating control unit was applied to heat the cell and control the cell temperature. An ARBIN FCTS LNR was used to supply required electric loads to the cell.

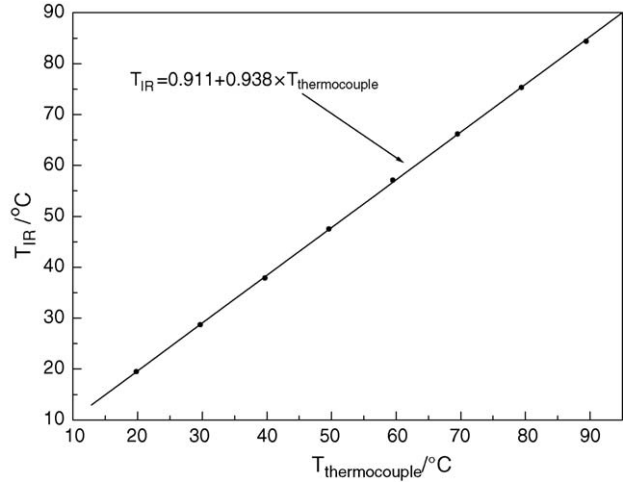

Fig. 3. Correlation of the temperatures measured with the thermo tracer and the thermocouple.

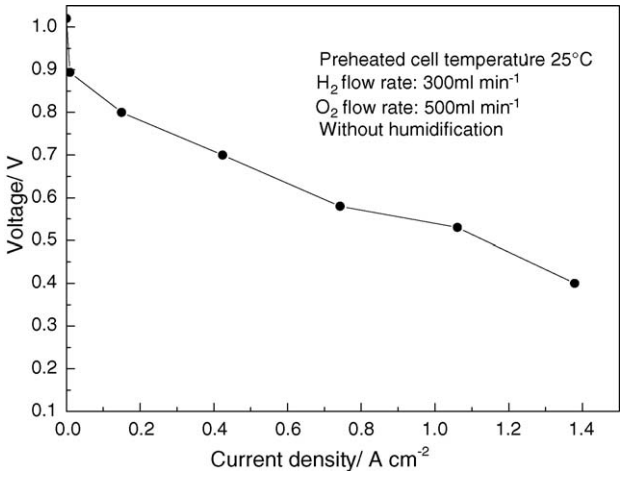

Fig. 4. Polarization curve of the test cell without humidification.

A T-type thermocouple was inserted into the middle of the cathode flow field plate to monitor the temperature, which is taken as the cell temperature in this paper. A heating pad was installed behind the cathode flow field plate to preheat the cathode flow field plate to an initial temperature. The initial temperature before loading current is called preheated cell temperature in this paper.

In order to avoid the appearance of liquid water in the anode side, dry oxygen and hydrogen without preheating were supplied in our experiments. The atmospheric temperature was 14 °C. A polarization curve showing the performance of the test cell without humidification is shown in Fig. 4.

3. Results and discussion

The typical images of temperature fields over the MEA anode side at different current densities are shown in Fig. 5. The inlet is the upper left corner and the outlet is the lower right corner. Each photo is taken at 60 s after loading current. The flow rates of hydrogen and oxygen are 300 and 500 ml min^{-1}, respectively. As seen, the temperature of the MEA surface increases with the current density. That is the result of the fact that heat generation increases with cell current density [4]. Also, the downstream temperatures are higher than the upstream in those images. In this case, because the dry reactants are supplied in experiments, all the water needed in the membrane and the anode come from the cathodal product of the electrochemical reactions. As a result, both the membrane hydration and water activity in the anode increase along the flow path. Proton conductivity of the solid polymer membrane depends on the rate of hydration [17]. Therefore, the local current increases along the channel, which leads to higher temperatures at downstream. The hot spot (local higher temperature region) over the whole MEA's surface is easy to be located in these images. Knowing the position of hot spot by the method presented in this paper benefits to proper heat management and to suggest better cell design.

In order to compare in a chart temperature fields under different operating conditions, the temperatures at 27 points in the flow field, as shown in Fig. 6, were taken from visualized temperature

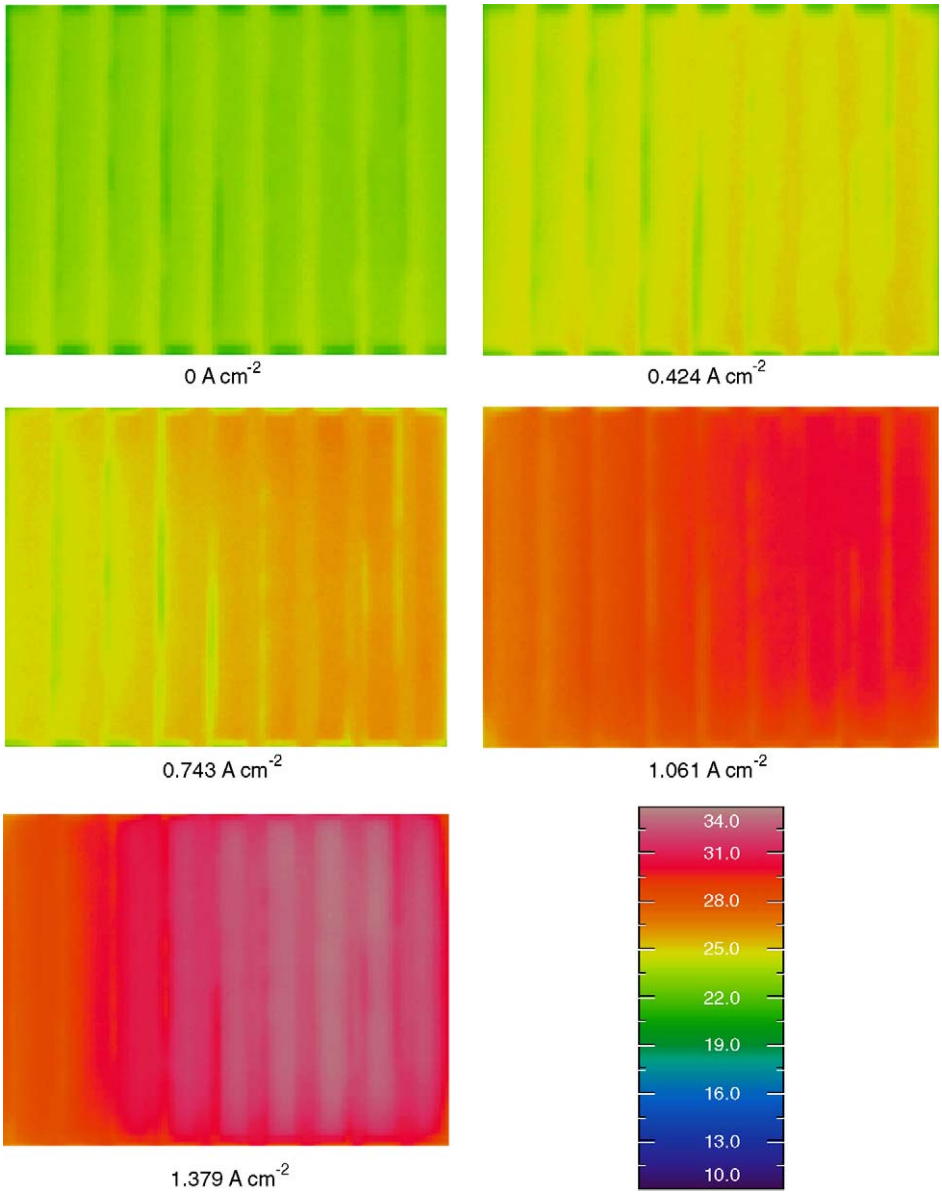

Fig. 5. Images of temperature fields on the MEA surface at different current densities.

fields and converted with the equation shown in Fig. 3. Fig. 6 also shows the active area (39 mm × 29 mm), which is transparent for infrared.

Fig. 7 describes the effect of the loaded current density on the temperature field on the MEA surface. The data were taken from the images in Fig. 5. As can be seen, both the temperatures and non-uniformity of temperature distribution over the surface increase with the loaded current density. At high current densities, the temperatures at the outlet points are not the highest in the temperature field. Although the hydration of the membrane at the outlet area is the highest, the depletion of oxygen due to oversaturation of vapor and the accumulated liquid water at the cathode side will weaken the mass transportation to the catalyst layers, which will lead to lower local current densities [18]. As a result, the temperatures at outlet regions decrease slightly.

Fig. 8 shows the plot of the temperature rise with current density. As shown, the average temperature of the MEA surface increases with the current density. With the increase of current density, more reactants react and the cell voltage (efficiency) decreases, and thus waste heat increases. Compared with the MEA temperature, the cell temperature increases slowly. For the convective heat transfer between the reactants and the MEA surface and heating from the cathode side, the mean temperature of MEA anode surface is lower than the cell temperature before loading current. With increasing of current density, the mean temperature of the MEA surface exceeds the cell temperature and the gap between them widens. This means that the heat generated by reactions cannot be radiated to environment quickly through the cell. A material with higher conductive heat coefficient is helpful to decrease the temperature gradient between the MEA and ambient.

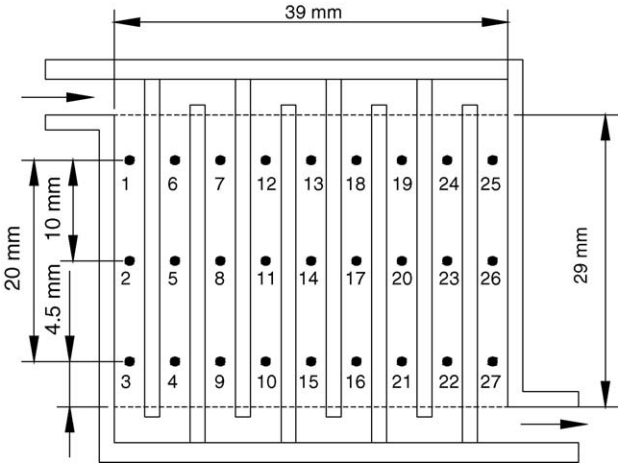

Fig. 6. The positions of the temperature points taken from the visualized temperature field.

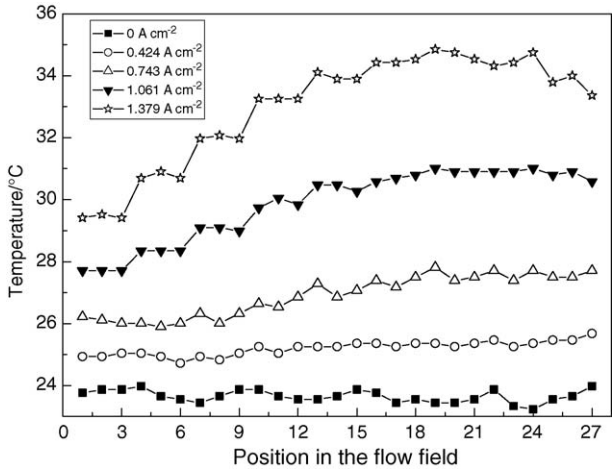

Fig. 7. The effect of current density on the temperature distribution over the MEA surface.

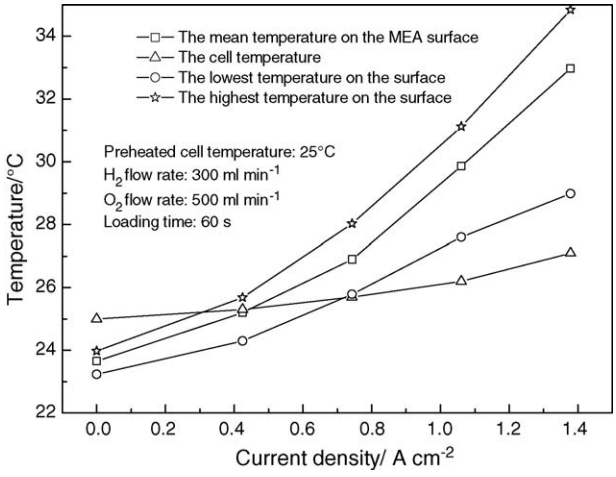

Fig. 8. The variations of the MEA temperature and the cell temperature with the current density.

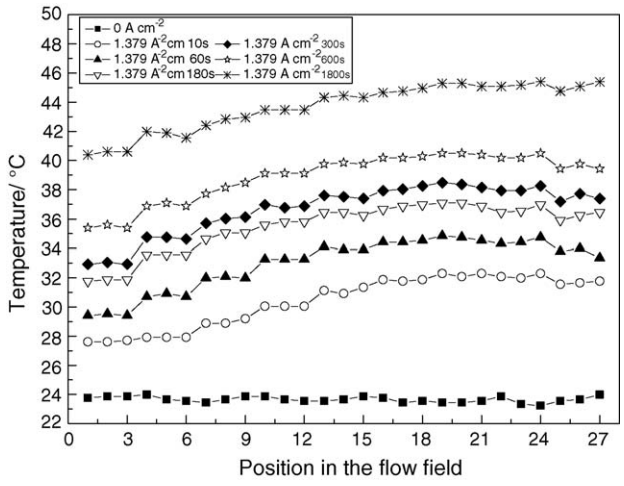

Fig. 9. The effect of loading time on the temperature field of the MEA surface.

As seen from Fig. 8, both the lowest and highest temperatures on the surface increase with current density. However, the highest temperature increases faster than the lowest temperature, which leads to the increase of the maximum temperature difference with the current density. Compared with the low temperature region, higher water activity and membrane hydration at the high temperature region make the local current density increase more when a higher current is loaded to the cell. Therefore, increasing the loaded current density would deteriorate the current distribution, and then deteriorates the species and temperature distributions. These characteristics indicate that the temperature management inside PEMFCs becomes more serious and more attention should be paid for the application of higher loaded current densities.

The change of temperature field with loading time at constant current density of 1.379 A cm^{-2} is presented in Fig. 9. All the temperatures at selected 27 points increase with loading time. The basic contour of temperature distribution has formed at 10 s after loading current. Fig. 10 shows the variations of temperatures of the MEA surface and cell with the loading time. As shown, the average temperature of the surface increases with the loading time within 1800 s. The reason is that the heat generated

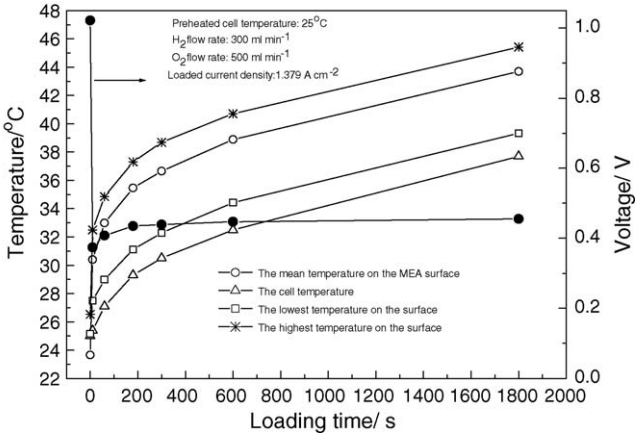

Fig. 10. The variations of the MEA temperature and cell temperature with loading time.

by electrochemical reactions cannot radiate quickly through the test cell to environment. The time of 1800 s is not enough to reach a heat balance between the cell and environment. In other words, the cell's ability to remove heat is not good. The cell voltage becomes stable after a loading time of about 180 s. The difference between the MEA mean temperature and the temperature of cathode flow field plate no longer changes after an initially sharp increase with period of about 180 s. It implies that the heat conduction between the MEA and the cathode flow field plate becomes stable after 180 s. However, the heat transfer between the cell and the environment is still unstable within 1800 s because both the MEA and cell temperatures increase continuously. It is implied that the stabilization of electrical performance of the cell does not stand for the heat transfer balance achieved inside the cell. The change of MEA's temperature should be monitored for safe operating of the cell. Temperature variations of the MEA and the cathode flow field plate within 1800 s are shown to be about 20 and 13 °C, respectively. The increase with loading time of the highest temperature and the lowest temperature over the surface is also shown in Fig. 10. At the beginning after loading current, the highest temperature increases much faster than the lowest temperature because the highest local current density at location where highest temperature occurs produces much more heat after loading current. The difference between the highest temperature and the lowest temperature tends to be stable after initial 300 s. From the results and discussion on the temperature change with loading time, it is recognized that the heat transfer processes inside PEMFCs needs much longer time to reach stabilization than the electrochemical processes. The change of temperature distribution of MEA surface after loading current is important because it is related to cell start-up and changing load for practical application. Learning the feature of temperature distribution change with loading time is necessary for safe start of a PEMFC. The experimental results of temperature field change after loading can help the safe starting and operating of the cell.

The non-uniformity of temperature field over the MEA surface and the big variation of MEA and cell temperatures with the loaded current and loading time indicate that the assumption of isothermal temperature distribution is not appropriate for modeling purposes in PEMFCs. The gap between MEA temperature and the cell temperature and the non-uniformity of temperature field over the MEA surface also reveal that monitoring the temperature of external surface of the flow field plate or end plate cannot supply an accurate reference to control the MEA's temperature. So, it is essential to explore the detailed heat transfer processes inside PEMFCs with experiments and numerical simulations. Novel methods need to be found to effectively monitor the temperatures of the MEA.

4. Conclusions

With the new designed PEMFC with serpentine flow bed and infrared imaging technology, the temperature distributions on the anode surface of the MEA were studied experimentally under non-humidification conditions. The results enrich our knowledge of temperature distribution and heat transfer inside PEMFCs. Knowing the knowledge is helpful to improve cell design and operation, to proper water/heat management and to validation the numerical modeling of PEMFCs. The following conclusions can be drawn from this work:

(1) The temperature distributions over the MEA surface under whole channel region were achieved. In the serpentine flow field, under non-humidification, the downstream temperatures are higher than the upstream over the MEA surface because of the increase of membrane hydration, and the hot spot on the MEA surface is easy to locate from the infrared temperature image.
(2) The MEA's mean temperature, the cell temperature and non-uniformity of temperature distribution all increase with the current density. The increase of cell temperature is slower than that of the mean temperature on the MEA surface.
(3) After loading a constant current density of 1.379 A cm^{-2}, the MEA temperature and the cell temperature increase with loading time within 1800 s. The maximum temperature difference tends to be stable after an initial 300 s sharp increase. The gap between the MEA mean temperature and the cell temperature no longer changes after an initial increase with time of 180 s.
(4) The experimental results indicate that an isothermal assumption is not accurate enough for modeling purposes in PEMFCs. Monitoring the temperature of external surface of flow field plate or end plate cannot supply an accurate reference to control the temperatures over the MEA surface.

Acknowledgements

This work was supported by National Natural Science Foundation of China (Grant Nos. 50236010, 50406010 and 50028605), Sino-German Center for Research Promotion of DFG and NSFC (Grant No. GZ207(101/7)) and Scientific Research Foundation for Doctors of Beijing University of Technology (52005014200401). The authors are grateful to Mr. Jielin Jia, Mr. Xuan Liu and Mrs. Yan Wang for their help and discussion, and to Peter King, P. Eng. for editing.

References

[1] H. Guo, C.F. Ma, M.H. Wang, J. Yu, X. Liu, F. Ye, C.Y. Wang, Proceedings of First International Conference on Fuel Cell Science Engineering and Technology, Rochester, NY, April 2003, pp. 471–476.
[2] M.M. Mench, Q.L. Dong, C.Y. Wang, J. Power Sources 124 (2003) 90–98.
[3] M.H. Wang, H. Guo, C.F. Ma, F. Ye, J. Yu, X. Liu, Y. Wang, C.Y. Wang, Proceedings of First International Conference on Fuel Cell Science Engineering and Technology, Rochester, NY, April 2003, pp. 95–100.
[4] M.M. Mench, D.J. Burford, T.W. Davis, Proceedings of ASME International Mechanical Engineering Congress & Exposition, Washington, DC, November 2003, pp. 415–428.
[5] A. Hakenjos, H. Muenter, U. Wittstadt, C. Hebling, J. Power Sources 131 (2004) 213–216.
[6] W.-K. Lee, S. Shimpalee, J.W. Van Zee, J. Electrochem. Soc. 150 (2003) 341–A348.
[7] D. Natarajan, T.V. Nguyen, J. Power Sources 115 (2003) 66–80.
[8] S. Shimpalee, S. Dutta, Numerical Heat Transfer Part A 38 (2000) 111–128.

[9] A. Rowe, X.G. Li, J. Power Sources 102 (2001) 82–96.
[10] K. Danenberg, P. Ekdunge, G. Lindbergh, J. Appl. Electrochem. 30 (2000) 1377–1387.
[11] N. Djilali, D.M. Lu, Int. J. Therm. Sci. 41 (2002) 29–40.
[12] T. Berning, D.M. Lu, N. Djilali, J. Power Sources 106 (2002) 284–294.
[13] G. Ju, J. Fan, S. Chen, Y. Liu, K. Cen, J. Power Sources 136 (2004) 1–9.
[14] P.J.S. Vie, S. Kjelstrup, Electrochim. Acta 49 (2004) 1069–1077.
[15] R. Schimoi, M. Masude, K. Fushinobu, Y. Kozawa, K. Okazaki, J. Energy Resour. Technol. 126 (2004) 258–261.
[16] S.D. Knights, C.M. Colbow, J.S. Pierre, D.P. Wilkinson, J. Power Sources 127 (2004) 127–134.
[17] M. Noponen, T. Mennola, M. Mikkola, T. Hottinen, P. Lund, J. Power Sources 106 (2002) 304–312.
[18] K. Dannenberg, P. Ekdunge, G. Lindbergh, J. Appl. Electrochem. 30 (2000) 1377–1387.